Anatase TiO2 nanosheet : an ideal host structure for fast and efficient lithium insertion/extraction

Chen, Jun Song; Lou, David Xiong Wen

2009

Chen, J. S., & Lou, D. X. W. (2009). Anatase TiO2 nanosheet : an ideal host structure for fast and efficient lithium insertion/extraction. Electrochemistry communications, 11(12), 2332-2335.

https://hdl.handle.net/10356/95584

https://doi.org/10.1016/j.elecom.2009.10.024

Anatase TiO_2 nanosheet: An ideal host structure for fast and efficient lithium insertion/extraction

Jun Song Chen, Xiong Wen Lou *

School of Chemical and Biomolecular Engineering,
Nanyang Technological University, 70 Nanyang Drive,
Singapore 637457, Singapore
** Corresponding author. Tel.: +65 6316 8879; fax: +65 6791 1761.*
E-mail address: xwlou@ntu.edu.sg (X.W. Lou).

A B S T R A C T

Anatase TiO_2 nanosheets with largely exposed (0 0 1) facets have been synthesized by a modified method. Exploitation of these nanosheets as a host structure for reversible lithium insertion/extraction has been investigated. It is found that these TiO_2 nanosheets manifest much lower initial irreversible losses compared to other anatase TiO_2 nanostructures, and excellent cycling performance at a charge–discharge rate as high as 20 C. The superior reversible lithium storage capability can be attributed to the ultrathin nano-sheet structure: a large exposed effective area and a very short diffusion path. It thus attests the promising use of these anatase TiO_2 nanosheets in high-power lithium–ion batteries.

1. Introduction

Titanium oxide (TiO_2) is probably the most widely studied semiconducting metal oxides due to its great application potential in many fields, such as photocatalysis, sensors, solar cells, and lithium–ion batteries [1–5]. For example, anatase TiO_2 has long been studied as a lithium insertion host material because of its crystal structure which can be viewed as a stacking of zigzag chains consisting of highly distorted edge-sharing TiO_6 octahedra [6]. This special 3D arrangement creates open channels which facilitate the insertion/extraction of Li^+ during discharge/charge [7]. In a TiO_2/Li half-cell, the principal reaction that governs the electro-chemical processes is as follows:

$$TiO_2 + xLi^+ + xe^- \leftrightarrow Li_xTiO_2 \qquad (1)$$

As studied previously, the maximum number of Li^+ that can be inserted is determined to be 0.5 [6], leading to a theoretical capacity of 167.5 mA h g^{-1} [8].

Very recently, anatase TiO_2 nanocrystals/nanosheets with large fraction of exposed high-energy (0 0 1) facets have been successfully synthesized in different reaction systems following the first report by Yang et al. (Nature 2008, 453, 638) [9–15]. Among them, hydrofluoric acid (HF) appears to be a very effective capping agent, as element F has a low F–F bonding energy [16] but bonds strongly to Ti atom [13], thus stabilizing the highly reactive (0 0 1) facets. Based on these methods, the percentage of exposed reactive (0 0 1) facets in the as-prepared TiO_2 crystals has been reported to be 47% [13], 60% [17], 80% [15], and even 89% [10]. Because of these highly

active crystal facets, their photocatalytic activities have been shown indeed superior by different groups [11,15,17]. However, to the best of our knowledge, there has been no report on the lithium storage properties of these anatase TiO_2 nanosheets. It is thus intriguing to investigate the potential use of these TiO_2nanosheets in lithium–ion batteries (LIB). Inspired by this idea, herein we investigate the lithium storage capabilities of the anatase TiO_2 nanosheets with exposed high-energy (0 0 1) surfaces. The TiO_2 nanosheets are synthesized following a recently reported method with slight modification, and the electrochemical results indicate that these nanosheets exhibit much lower initial irreversible capacity losses compared to other conventional anatase TiO_2 nanocrystals, and excellent capacity retention upon prolonged cycling.

2. Experimental

2.1. Material preparation

Pure anatase TiO_2nanosheetswith largely exposed (0 0 1) facets are synthesized through a modified hydrothermal method [10]. In a typical synthesis, 5 mL of titanate isopropoxide (97%, Sigma–Aldrich) was added into a 40 mL Teflon-lined autoclave. Then 0.6 mL of 48% HF solution was added drop-wise. After that, the mixed solution was sealed and put into an electric oven heated at 180 ℃ for 24 h. It was cooled down naturally to room temperature. The white precipitate was collected and washed with ultra-pure water several times before drying at 60 ℃ overnight. Anatase TiO_2 nanospheres (200 nm in diameter) were prepared by annealing amorphous TiO_2 nanobeads synthesized following a reported protocol with little modification [18] at 600 ℃ in air.

2.2. Material characterization

The chemical composition of products was confirmed by X-ray powder diffraction (Bruker, D8 – Advance X-ray Diffractometer, Cu Kα, λ= 1.5406 Å). Morphology and structure of the samples were examined by transmission electron microscope (JEOL, JEM-2100F, 200 kV) and field-emission scanning electron microscope (JEOL, JSM-6700F, 5 kV) equipped with energy-dispersive X-ray spectroscopy (EDX) analysis.

2.3. Electrochemical measurements

The electrochemical tests were performed using two-electrode Swagelok-type cells with lithium serving as both the counter and reference electrodes under ambient temperature. The working electrode was composed of 70 wt.% of active material (e.g., TiO_2 nanosheets), 20 wt.% of conductivity agent (carbon black, Super-P-Li), and 10 wt.% of binder (polyvinylidene difluoride, PVDF, Aldrich). The electrolyte used was 1 M $LiPF_6$ in a 50:50 (w/w) mixture of ethylene carbonate and diethyl carbonate. Cell assembly was carried out in an Argon-filled glovebox with both moisture and oxygen contents below 1 ppm. Cyclic voltammetry (CV, 1–3 V, 0.1 mV/s) was performed using an electrochemical workstation (CHI 660C). Galvanostatic charge/discharge was conducted using a battery tester (NEWAER) with a voltage window of 1–3 V at different current rates of 1 C, 4 C, and 10 C where 1 C = 167.5 mA g^{-1}.

3. Results and discussion

Fig. 1 shows the material characterization results of the as-prepared TiO_2 nanosheets. It can be clearly seen from the transmission electron microscopy (TEM) images (Fig. 1A and B) and the field-emission scanning electron microscopy (FESEM) image (Fig. 1C) that the nanosheets are generally rectangular or square-shaped with the edge length in the range of 20–100 nm. The thickness is about 10 nm, which is about twice the thickness of the nanosheets prepared in the original report [10]. This should be considered advantageous for reversible lithium insertion/extraction as the as-prepared TiO_2 nanosheets are more robust against the volume change during charge/discharge cycles. It was confirmed previously that the top and bottom facets of the nanosheets are the (0 0 1) planes [10]. Based on the above observed average dimensions, the percentage of exposed (0 0 1) facets is estimated to be about 62%. The crystal structure of the sample is confirmed by the X-ray diffraction (XRD) pattern (Fig. 1D). All the identified peaks can be unambiguously assigned to tetragonal anatase TiO_2 (JCPDS No. 21-1272, S.G.: $I4_1/amd$, a_o = 3.7852 Å, c_o = 9.5139 Å).

A series of electrochemical measurements are carried out in order to study the lithium storage capabilities of these as-prepared TiO_2 nanosheets. Fig. 2A shows the representative cyclic voltammograms (CV). Consistent with previous reports [19,20], two well-defined current peaks are observed at about 1.75 V and 2.1 V during cathodic and anodic sweeps, respectively. The cathodic peak at 1.75 V marks the two-phase transition of the structure from tetragonal anatase ($I4_1/amd$) to orthorhombic $Li_{0.5}TiO_2$(*Imma*) when the insertion coefficient x in reaction (1) has reached about 0.05 [8]. The corresponding anodic peak with almost the same current intensity shows that the Li^+ extraction takes place to the equal extent, indicating a nearly perfect Coulombic efficiency. It can also be observed that the current of both peaks increases in the subsequent cycles, indicating a possible activation process in the electrode material. Furthermore, there is no substantial change in the peak positions after the first scan, showing the high reversibility of the insertion/extraction reactions.

Fig. 2B shows the charge/discharge voltage profiles of the first two cycles at a high current drain of 4 C-rate. Remarkably, after reaching a high first discharge capacity of 164.8 mA h g^{-1} (almost equals the theoretical capacity of 167.5 mA h g^{-1}), a reversible capacity of 147.1 mA h g^{-1} can be delivered in the subsequent charge process. This corresponds to an irreversible capacity loss of only 10.7%. The sample has been discharged/charged at other C-rates, and the initial irreversible loss is generally in the range of 5–15%. This is in good agreement with the CV analysis, and should be regarded as very small for anatase TiO_2 materials. It has been reported in previous studies that the initial irreversible capacity loss is usually in the range of 30–40% for anatase phase TiO_2 nanotubes [20,21] and hollow micro/nanostructures [8,19]. One possible reason for such a significantly reduced irreversible loss of the as-prepared TiO_2 nanosheets might be attributed to its unique structure. Specifically, the largely exposed (0 0 1) facets provide more accessible sites for Li^+ insertion, and the ultrathin feature (ca. 10 nm) facilitates the efficient extraction. Furthermore, it is important to mention that the surface of TiO_2 nanosheets is stabilized by the F atoms introduced in the present synthetic system. Energy-dispersive X-ray (EDX) analysis indicates an atomic ratio (F/Ti) of about 0.21. It has been reported that the doping of F will decrease the bandgap of the active material [22], hence increasing the electronic conductivity. The second cycle gives a slightly lower discharge capacity of 151.6 mA h g^{-1}, and the charge capacity is 146.5 mA h g^{-1}, leading to an irreversible loss of only 3.4%.

Fig. 2C shows the cycling performance of the as-prepared TiO_2 nanosheets at different current rates of 10 C and 20 C. It can be clearly seen that the cycling performance at a 20 C-rate is very close to the 10 C-rate one, indicating the high efficiency of solid state diffusion of Li^+ in these TiO_2 nanosheets. At the end of 200 charge/discharge cycles, a reversible capacity of 120.2 mA h g^{-1} and 111.8 mA h g^{-1} can still be retained for 10 C and 20 C cycling, respectively. These values suggest that the as-synthesized TiO_2 nanosheets manifest excellent high rate performance.

In order to further understand the origin of the outstanding lithium storage capabilities of these TiO_2 nanosheets, some comparative studies were carried out with the results shown in Fig. 3. Fig. 3A displays the morphology of anatase TiO_2 nanospheres of ~200 nm in size. The comparative cycling performances of TiO_2 nanosheets, nanospheres, as well as commercially available Degussa P25 nanoparticles are shown in Fig. 3B. Apparently, the as-prepared TiO_2 nanosheets deliver a much higher capacity than the other two TiO_2 samples throughout the cycling. We further compare the performance of TiO_2 nanosheets to that of anatase TiO_2 hollow nanostructure synthesized using TiF_4 as the TiO_2 precursor [8]. Since both materials have their surface stabilized by F atoms, this might suggest that the superior lithium storage capabilities of TiO_2 nanosheets arise mainly from the unique structure.

4. Conclusions

In conclusion, anatase TiO_2 nanosheets with a thickness of about 10 nm are synthesized in large scale through a modified hydrothermal method. They possess large percentage of exposed (0 0 1) facets. When evaluated for lithium storage capabilities, these as-prepared TiO_2 nanosheets exhibit excellent performance. It shows a significantly lower initial irreversible capacity loss compared to other anatase TiO_2 materials. This has been attributed to its unique nanostructure which could facilitate efficient lithium insertion and extraction. The TiO_2 nanosheets also demonstrate excellent capacity retention after prolonged cycling at a 20 C-rate. The present study suggests that these interesting anatase TiO_2 nanosheets are very promising as anode materials for high-power lithium–ion batteries.

Acknowledgements

We are grateful to the Nanyang Technological University for financial support through the start-up grant (SUG).

References

[1] D.H. Chen, F.Z. Huang, Y.B. Cheng, R.A. Caruso, Adv. Mater. 21 (2009) 2206.
[2] A. Fujishima, K. Honda, Nature 238 (1972) 37.
[3] M. Gratzel, Nature 414 (2001) 338.
[4] H.J. Snaith, L. Schmidt-Mende, Adv. Mater. 19 (2007) 3187.
[5] K. Yong Joo, L. Mi Hyeon, K. Hark Jin, L. Gooil, C. Young Sik, P. Nam-Gyu, K. Kyungkon, L. Wan In, Adv. Mater. 21 (2009) 3668.
[6] G. Nuspl, K. Yoshizawa, T. Yamabe, J. Mater. Chem. 7 (1997) 2529.
[7] D. Deng, M.G. Kim, J.Y. Lee, J. Cho, Energy Environ. Sci. 2 (2009) 818.
[8] X.W. Lou, L.A. Archer, Adv. Mater. 20 (2008) 1853.
[9] Y.Q. Dai, C.M. Cobley, J. Zeng, Y.M. Sun, Y.N. Xia, Nano Lett. 9 (2009) 2455.
[10] X. Han, Q. Kuang, M. Jin, Z. Xie, L. Zheng, J. Am. Chem. Soc. 131 (2009) 3152.
[11] B.H. Wu, C.Y. Guo, N.F. Zheng, Z.X. Xie, G.D. Stucky, J. Am. Chem. Soc. 130 (2008) 17563.
[12] H.G. Yang, G. Liu, S.Z. Qiao, C.H. Sun, Y.G. Jin, S.C. Smith, J. Zou, H.M. Cheng, G.Q. Lu, J. Am. Chem. Soc. 131 (2009) 4078.
[13] H.G. Yang, C.H. Sun, S.Z. Qiao, J. Zou, G. Liu, S.C. Smith, H.M. Cheng, G.Q. Lu, Nature 453 (2008) 638.
[14] G. Liu, H.G. Yang, X. Wang, L. Cheng, J. Pan, G.Q. Lu, H.-M. Cheng, J. Am. Chem. Soc. 131 (2009) 12868.
[15] D.Q. Zhang, G.S. Li, X.F. Yang, J.C. Yu, Chem. Commun. (2009) 4381.
[16] K.F. Zmbov, J.L. Margrave, J. Phys. Chem. 71 (1967) 2893.
[17] G. Liu, H.G. Yang, X. Wang, L. Cheng, J. Pan, G.Q. Lu, H.-M. Cheng, J. Am. Chem. Soc. 131 (2009) 12868.
[18] Y.J. Kim, M.H. Lee, H.J. Kim, G. Lim, Y.S. Choi, N.-G. Park, K. Kim, W.I. Lee, Adv. Mater. 21 (2009) 3668.
[19] B. Song, S. Liu, J. Jian, M. Lei, X. Wang, H. Li, J. Yu, X. Chen, J. Power Sources 180 (2008) 869.
[20] J. Xu, C. Jia, B. Cao, W.F. Zhang, Electrochem. Acta 52 (2007) 8044.
[21] X.P. Gao, Y. Lan, H.Y. Zhu, J.W. Liu, Y.P. Ge, F. Wu, D.Y. Song, Electrochem. Solid-State Lett. 8 (2005) A26.
[22] J.C. Yu, Yu Ho, Jiang Zhang, Chem. Mater. 14 (2002) 3808.

List of Figures

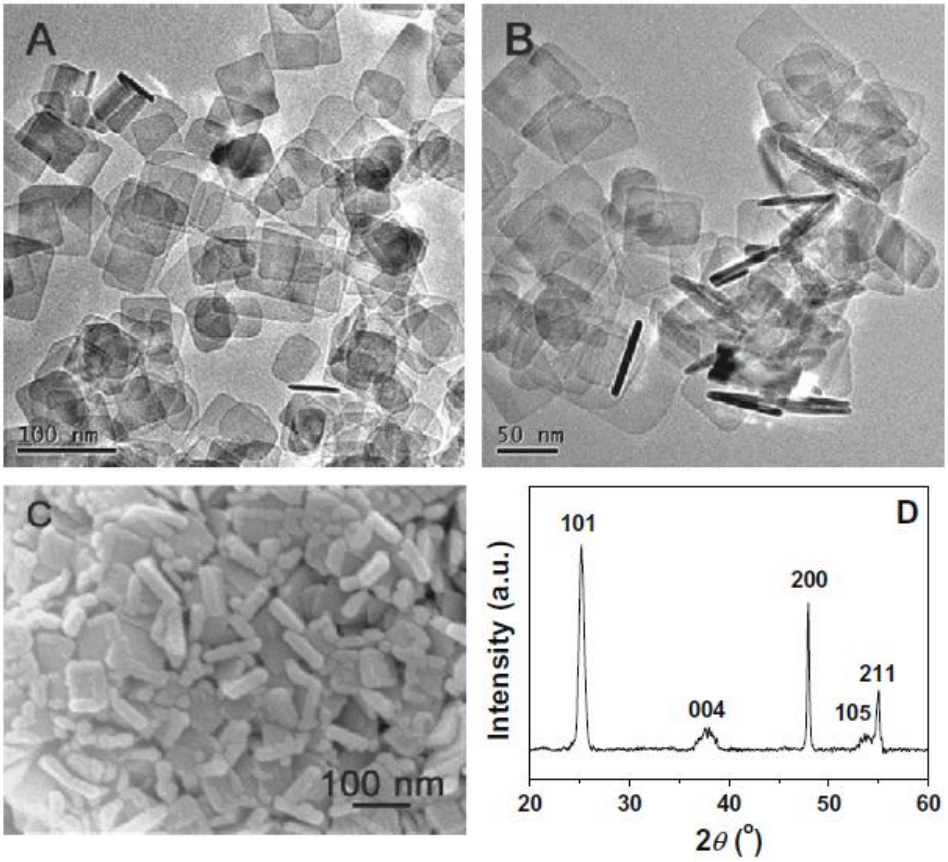
A
100 nm
B
50 nm
C
100 nm
D
101
200
004
211
105
Intensity (a.u.)
20
30
40
50
60
2θ (°)

Figure 1

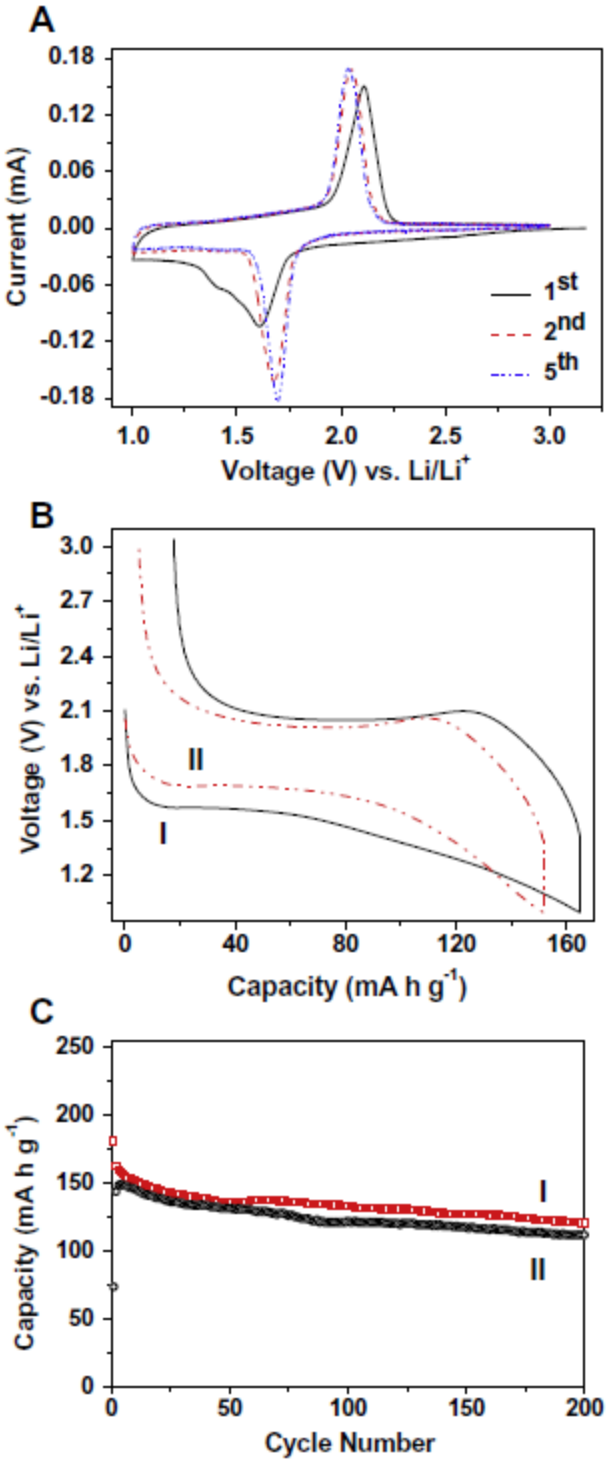
A
0.18
0.12
0.06
0.00
-0.06
-0.12
-0.18
Current (mA)
1.0
1.5
2.0
2.5
3.0
Voltage (V) vs. Li/Li+
1st
2nd
5th
B
3.0
2.7
2.4
2.1
1.8
1.5
1.2
Voltage (V) vs. Li/Li+
II
I
0
40
80
120
160
Capacity (mA h g-1)
C
250
200
150
100
50
0
Capacity (mA h g-1)
I
II
0
50
100
150
200
Cycle Number

Figure 2

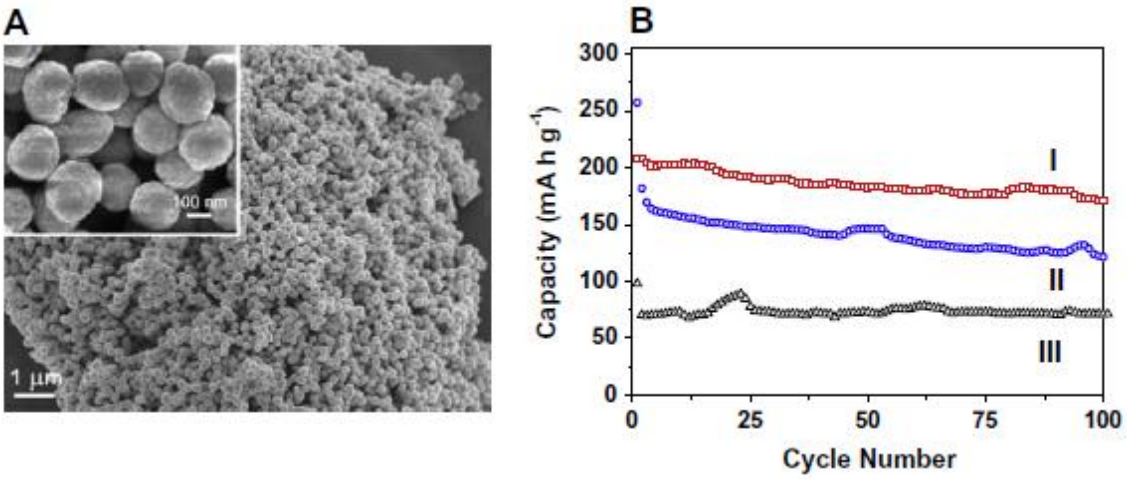
A
100 nm
1 μm
B
Capacity (mA h g-1)
Cycle Number
I
II
III
0
50
100
150
200
250
300
0
25
50
75
100

Figure 3